IEEE Access
Multidisciplinary ⋮ Rapid Review ⋮ Open Access Journal

Received September 22, 2021, accepted October 10, 2021, date of publication October 13, 2021, date of current version October 21, 2021.

Digital Object Identifier 10.1109/ACCESS.2021.3119698

Inline Waveguide Pseudo-Elliptic Filters Using Non-Resonating Modes With Folded-Waveguide Resonators

MUHAMMAD ANIS CHAUDHARY, (Member, IEEE), AND MUHAMMAD MANSOOR AHMED, (Senior Member, IEEE)
Department of Electrical Engineering, Capital University of Science and Technology, Islamabad 44000, Pakistan
Corresponding author: Muhammad Anis Chaudhary (anisch@ieee.org)

ABSTRACT In this paper, a new structure to implement inline waveguide pseudo-elliptic filters using folded-waveguide (FWG) resonators along with non-resonating modes has been proposed. The basic structure is an FWG resonator fed by a rectangular waveguide through inductive irises. The $\boldsymbol{TE_{10}}$ mode of the feeding rectangular waveguide excites both dominant and first higher order modes in the FWG structure. The dominant mode of the FWG acting as a non-resonating mode creates an alternate energy path from source to load thus producing a transmission zero (TZ), while the first higher order mode acts as the resonant mode resulting in a pole. The structure therefore acts as a singlet capable of realizing a pole and a TZ either below or above the passband depending on the offset of the feeding irises from the center of the FWG resonator and relative to each other. The structure also provides flexibility in shifting the FWG center axis relative to the feeding rectangular waveguides, thus giving more coupling control and realizing wider range of singlet responses. The proposed singlet structure does not require any increase in the cross-sectional size relative to the standard rectangular waveguide. Two prototype filters using the proposed singlet structures have been designed, manufactured and tested. Measurements show good agreement with the simulations, verifying the feasibility of the proposed structure.

INDEX TERMS Waveguide filters, pseudo-elliptic response, transmission zeros, bandpass filters.

I. INTRODUCTION

Pseudo-elliptic bandpass filter responses can implement a sharper transition from passband to stopband because of their ability to realize finite frequency transmission zeros (TZs) and are therefore preferred by modern microwave transceivers [1], [2]. For applications requiring low losses and/or high power handling capability, these filters are implemented in waveguide technology [3]. Several methods for realization of TZs in waveguide technology have been proposed in the literature, including cross-coupling between non-adjacent resonators and the use of multi-mode cavities [3]–[9], extracted pole synthesis method [10] and the use of inverters based on frequency-dependent coupling sections [11]. A relatively new approach of realizing pseudo-elliptic response that has attracted attention in the last decade is the use of non-resonating modes to create additional energy paths [1], [12], [13]. The non-resonating modes can either be propagating or evanescent at the passband of the filter and they can provide additional energy paths and thus can be used to implement arbitrarily located finite frequency transmission zeros (TZ) while still keeping the inline topology. In this regard, the earliest work makes use of asymmetric irises in a rectangular waveguide [14], [15] to realize TZs but the non-resonating (TE_{20}) mode vanishes very quickly along the cavity, resulting in week source to load coupling and thus the flexibility in terms of positioning of TZs is limited. To overcome this limitation, resonating mode of TE_{201} has been utilized in an enlarged width rectangular waveguide cavity [16]–[18] to realize the finite frequency TZs. A relatively compact singlet (A singlet [19] is a structure that produces a pole along with a transmission zero.) implementation is possible by using TM_{110} mode as the resonant mode [20]. To achieve further compactness, the concept of

The associate editor coordinating the review of this manuscript and approving it for publication was Andrei Muller.

TM dual-mode cavity has been combined with the idea of non-resonating modes [21]–[23].

The above mentioned techniques lead to an increase in the cross-sectional size relative to the standard all-pole waveguide iris filters. For applications where the increase in cross-section is undesirable, inline waveguide pseudo-elliptic filters capable of realizing finite frequency TZs can be implemented using the methods proposed in [24]–[28]. Pseudoelliptic waveguide filters can be realized by using rectangular ridge resonators as singlets [24], [25] to produce TZs below and/or above the passband. These filters can easily be manufactured using computer numerical control (CNC) milling of solid aluminum and do not require any additional components, making these structures economical and repeatable for production purposes. However, these advantages are achieved at the expanse of slightly lower unloaded quality factors in these filters. Pseudo-elliptic filters can also be implemented using dielectric disks appropriately located in a rectangular waveguide [26], [27]. However, for these filters to work, each dielectric resonator has to be precisely positioned at a certain angle in the waveguide leading to a tedious fabrication process. Pseudo-elliptic characteristic can also be realized by using dual post resonators [28] inside a rectangular waveguide. A TZ below the passband is achieved by having different post heights, while TZ in the upper stopband is implemented by using rotation of dual-post resonators. The dual-post resonators however have to be manufactured separately and then push fit (or screw fit) into the waveguide, thus making the manufacturing more involved.

In this paper, we introduce a new singlet structure for realization of inline waveguide pseudo-elliptic filters, using non-resonating modes with folded-waveguide (FWG) resonators. The singlet is comprised of an FWG resonator which is fed by input and output waveguide sections using inductive irises, as shown in Fig. 1. By adjusting the location of irises with respect to the FWG center axis, a TZ either below or above the pole can be implemented. Additionally the proposed singlet offers flexibility in adjusting the center axis of FWG relative to the center axis of feeding rectangular waveguides. The filters realized using these singlets, do not require any increase in the cross-sectional size with respect to the standard rectangular waveguide. Two prototype pseudo-elliptic filters are designed, manufactured and tested. The experimental results of these prototype filters are close to the simulations and thus validate the proposed singlet structure and the overall filter topologies.

Pseudo-elliptic filters presented in [16], [17] make use of TE_{201} mode as a resonant mode while the bypass coupling is provided by TE_{10} mode which acts as a non-resonating mode. To achieve a pole at the desired frequency in the passband the width of the rectangular cavity implementing TE_{201} has to be significantly increased beyond that of the feeding waveguide. The center of the enlarged width cavity can be easily adjusted relative to the center axis of the feeding waveguides to achieve flexibility in realization of the finite-frequency TZ at the desired location. A singlet structure presented in [29] and also explained in [13] again uses an enlarged width rectangular waveguide cavity but with TE_{301} mode as the resonating mode. The width dimension of the realized singlet is significantly larger than that of a standard rectangular waveguide. On the other hand, the singlet structure proposed in this paper combines an FWG resonator with the concept of non-resonating modes. The resonating mode used to excite the FWG is TE_{201} like mode while TE_{10} acts as the non-resonating mode. The main advantage of the proposed singlet arrangement over those presented in [16], [17], [29] is that the proposed structure does not require any increase in cross-sectional dimensions beyond those of a standard waveguide. However, the enlarged width cavity based singlets of [13], [16], [17], [29] do present great flexibly in setting the location of TZ at the required frequency by just adjusting the center of singlet cavity relative to the centers of feeding rectangular waveguides. This is easily achieved since these singlets are not constrained by the cross-sectional dimensions of the feeding waveguides. In contrast the FWG based singlet structure presented in this article, has to fit inside the normal cross-sectional size of a standard waveguide and therefore we cannot simply offset the whole FWG structure relative to the feeding waveguides. To address this constraint, we have introduced a dimension r which can be adjusted to effectively shift the FWG center axis relative to that of the feeding waveguide, as shown in Fig. 1 without any increase in cross-sectional size. To the best of our knowledge, this way of using an FWG structure with feeding irises to realize a singlet structure has not been reported before. The filters based on the oversized rectangular cavity singlets of [13], [16], [17], [29] may provide a good solution for implementations at THz and millimeter-wave frequencies because of the smaller wavelengths (and hence smaller cavity dimensions) involved at those high frequencies. However in the lower microwave spectrum (<30GHz), this increase in cross-sectional area makes the filter bulky and presents a limitation particularly in "retrofit" [13] applications where all-pole filters of a pre-existing microwave system need to be upgraded by better performance (pseudo-elliptic) but similar size filters. The filters designed using the singlet structures proposed in this paper may be good candidates for such applications because their cross-sectional dimensions would be the same as the pre-existing all-pole waveguide filters.

II. SINGLET BASED ON A FOLDED-WAVEGUIDE (FWG) RESONATOR

Folded-waveguide (FWG) structure can be thought of as a reduced height rectangular waveguide, folded at one or more suitable axis locations. The conceptual development of two commonly used FWG topologies in literature [30]–[33], is shown in Fig. 2. The equivalent reduced height rectangular waveguide along with electric field distribution of dominant (TE_{10}) and first higher order (TE_{20}) modes are shown in Fig. 2(a). Fig. 2(b) shows the FWG achieved by two foldings of the reduced height rectangular waveguide.

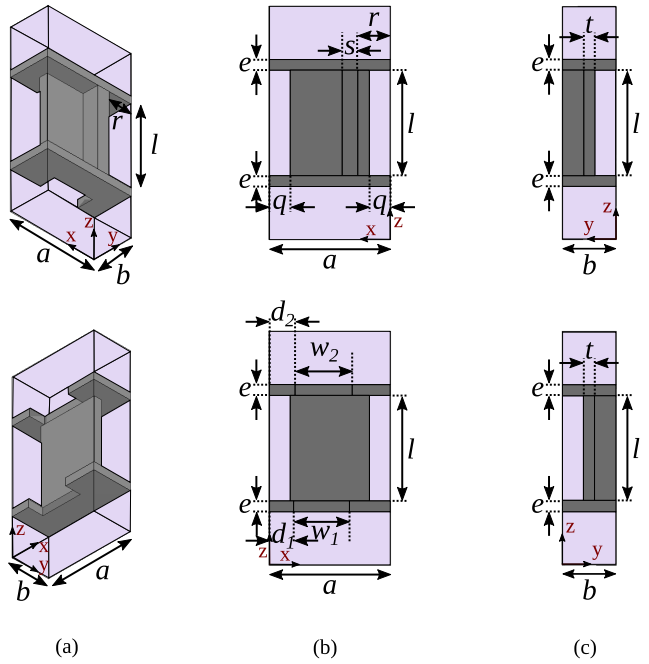

FIGURE 1. Different views of the proposed FWG-based singlet structure. (a) Perspective views, (b) top and bottom views, and (c) side views.

Fig. 2(c) is achieved by one folding at the center of the reduced height rectangular waveguide. Note that for both types of FWGs, the location of the FWG center axis is fixed and is marked by a cross in the Fig. 2.

In contrast to the conventional FWG shown in Fig. 2(b), we propose a slightly different FWG structure with a provision of adjusting the center axis of the FWG with respect to the feeding rectangular waveguide, thus offering more flexibility by allowing shifting of the dominant FWG mode electric field maximum relative to the feeding rectangular waveguide electric field maximum. The cross-sectional view of this proposed FWG structure is shown in Fig. 3, along with the electric field distribution of the first two modes. The parameter r can be used to adjust the location of the FWG center axis.

We propose a new singlet structure by using the FWG structure of Fig. 3 which is capable of realizing both a pole and a TZ either in the lower or in the upper stopband. The FWG is fed by input and output inductive irises from two rectangular waveguide sections which results in a singlet structure. Different views of this singlet are shown in Fig. 1. The cross-sectional views of different parts of the proposed singlet are shown in Fig. 4. The dominant TE_{10} mode of the feeding rectangular waveguide sections can excite both the dominant (TE_{10} like mode) and the first higher order (TE_{201} like mode) modes in an FWG section, thus resulting in a singlet capable of realizing a pole and a TZ. Whether the TZ is implemented below or above the passband depends on the location of irises with respect to the FWG center axis and with respect to each other.

Fig. 5 shows the top view of the singlet structure along with magnetic field lines for the resonating and the

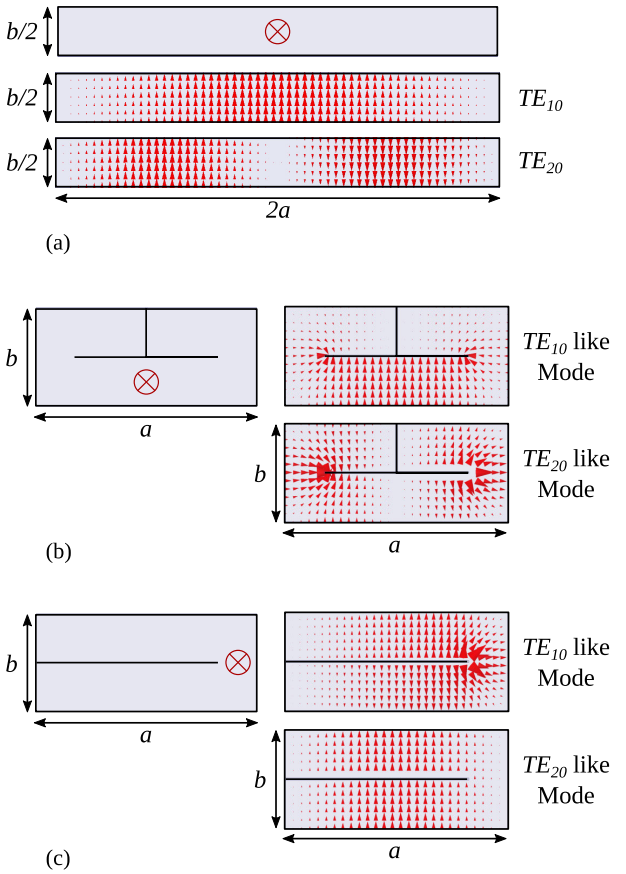

FIGURE 2. Conceptual development of conventional FWGs from an equivalent reduced height rectangular waveguide. (a) Reduced height rectangular waveguide, (b) FWG obtained by two foldings of the equivalent reduced height rectangular waveguide, and (c) FWG achieved by single folding at the center of the equivalent reduced height rectangular waveguide. Red arrows show the electric field distribution of first two modes in each type of waveguide. ⊗ denotes center axis for each type of waveguide.

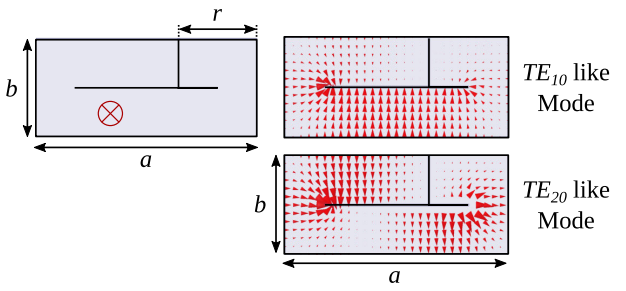

FIGURE 3. Proposed FWG with adjustable center axis. ⊗ denotes center axis of the proposed FWG structure. Red arrows indicate the electric field distribution for the dominant and the first higher order mode.

non-resonating modes. When both irises are at FWG center axis, resonating mode is not excited leading to only source to load coupling. When these irises are shifted away from the FWG center axis, the result is a pole and a TZ. A TZ is realized below the passband when the irises are on same side with respect to the FWG center while a TZ above the passband is implemented when the irises are located on opposite sides of the FWG center axis. It is worth mentioning that the proposed

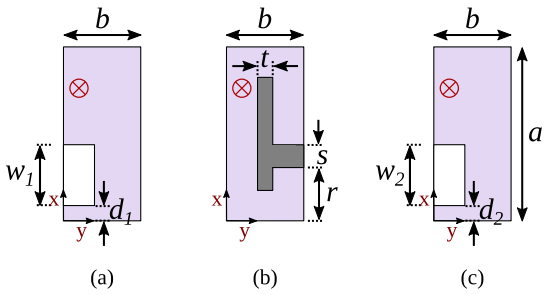

FIGURE 4. Cross-sectional views of the proposed singlet in the transverse plane. (a) Input iris, (b) FWG cavity, and (c) output iris. ⊗ denotes center axis of the FWG structure.

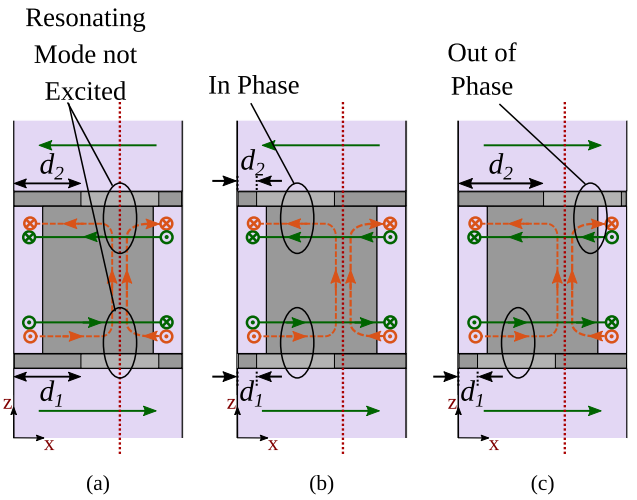

FIGURE 5. FWG-based singlet with irises: (a) Centered at FWG center axis, (b) on same side of FWG center axis, and (c) on opposite sides of FWG center axis. Dotted lines: FWG center axis. Dashed arrows: Magnetic field lines for TE_{201} like mode (resonating mode) in FWG. Solid arrows: Magnetic field lines for TE_{10} mode in rectangular waveguide and TE_{10} like mode (nonresonating mode) in FWG.

singlet structure can also be fed by FWG sections instead of rectangular waveguide sections.

The proposed singlet response can be represented by a 3×3 normalized coupling matrix (CM) given below [19].

$$M^{(Si)} = \begin{bmatrix} 0 & M_{S1} & M_{SL} \\ M_{S1} & M_{11} & M_{1L} \\ M_{SL} & M_{1L} & 0 \end{bmatrix} \tag{1}$$

The routing and coupling scheme for this singlet structure is given in Fig. 6. A TZ can be implemented at different locations from the proposed singlet by changing certain physical parameters of the structure, as explained in the cases below.

A. IRISES CENTERED AT THE CENTER AXIS OF FWG

In this case the feeding input and output irises are positioned at the center axis of FWG [see Fig. 5(a)]. As shown by the magnetic field lines of Fig. 5(a), the resonating mode of FWG (TE_{201} like mode) because of its odd symmetry cannot be excited by the even symmetry dominant TE_{10} mode of the

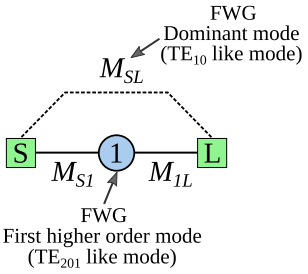

FIGURE 6. Routing and coupling scheme of the proposed FWG-based singlet.

rectangular waveguide and therefore does not create any pole or any TZ i.e. $M_{S1} = M_{1L} = 0$. Bypass coupling between source and load, however is non-zero ($M_{SL} \neq 0$), because the feeding rectangular waveguide does excite the dominant (TE_{10} like) mode of the FWG.

B. IRISES ON SAME SIDE OF FWG CENTER AXIS

When the centers of the two irises are shifted away from the FWG center axis and when both irises are located on the same side relative to the FWG center axis [see Fig. 5(b)], the feeding TE_{10} mode of the rectangular waveguide can excite both dominant and first higher order modes of the FWG, resulting in realization of a pole and a TZ. As shown in Fig. 5(b), the magnetic field lines for dominant mode of FWG are in phase with those of resonating (first higher order) mode of FWG at the cavity output and hence the TZ is realized below the passband. Note that this result is also consistent with the singlet implementation of [16]–[18], using an oversized rectangular waveguide cavity with TE_{201} as resonant mode.

As shown in Fig. 7, location of the resulting TZ can easily be varied by changing dimension d of input and output irises (here $d_1 = d_2 = d$). Additionally the parameter r can be used to shift the location of FWG center axis. This shift in location of FWG center axis is particularly useful for this case of same side irises, since it offers more flexibility in realization of required singlet response and since both irises are located on same side. All couplings ($M_{S1} \neq 0$, $M_{1L} \neq 0$ and $M_{SL} \neq 0$) are non-zero for this case.

Fig. 7(a) shows singlet response against variations in d, for $r = 4$ mm. The inset shows the cross-sectional views of the different portions of singlet structure, for $r = 4$ mm along with the location of FWG center axis. TZ below the passband is realized for $d = 1, 2, 3, \ldots 10$ mm. For d=11 mm, the two irises are very close to the FWG center axis, and therefore the resonating mode is not excited. Thus neither pole nor TZ is realized for d=11 mm.

Similarly, Fig. 7(b) and (c) shows the singlet responses for r=7 mm and r=10 mm, respectively. Note that Fig. 7 shows the responses for a singlet with dimensions d_1 of input iris and d_2 of output iris as equal and thus M_{S1}=M_{1L}, which is not essentially required by the singlet structure and thus these dimensions can be set independently to achieve the desired response.

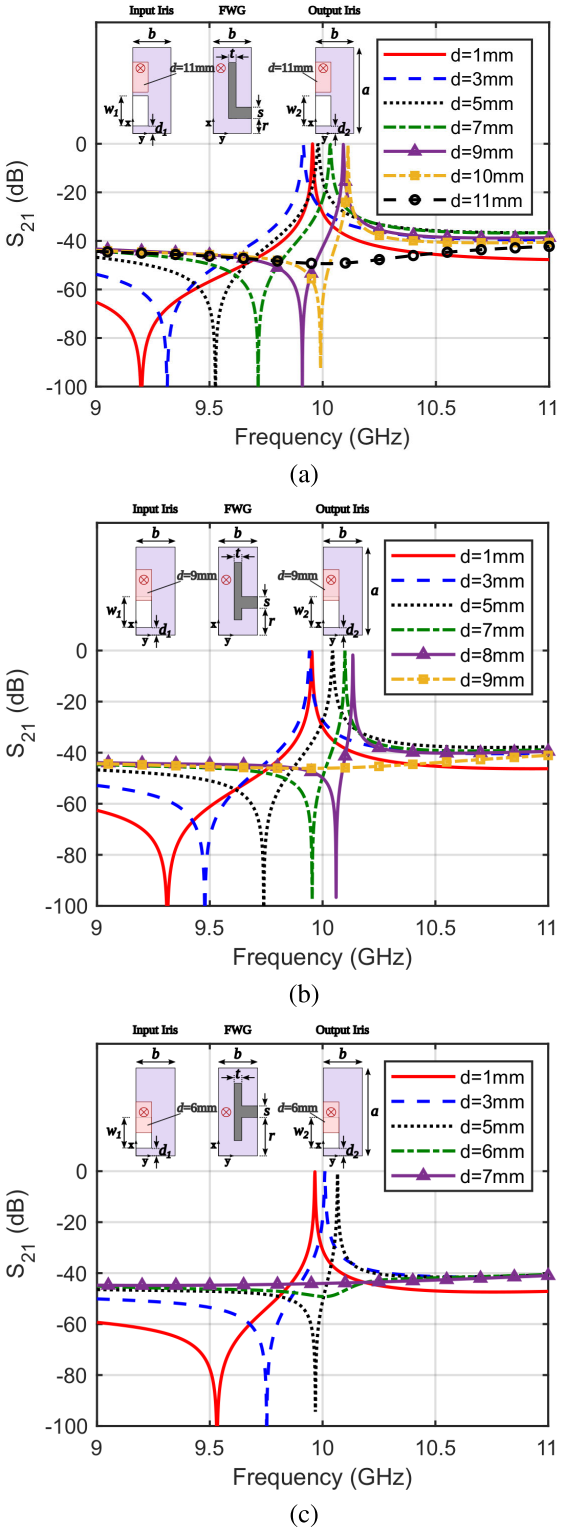

FIGURE 7. S_{21} versus d for the proposed singlet with irises on same side of FWG center axis for (a) $r = 4$ mm, (b) $r = 7$ mm, and (c) $r = 10$ mm. Insets of (a), (b) and (c) show the cross-sectional views of input iris, FWG cavity resonator and output iris for $r = 4$ mm, 7 mm and 10 mm respectively. ($a = 22.86$ mm, $b = 10.16$ mm, $d_1 = d_2 = d$, $w_1 = w_2 = 8$ mm, $t = 2$ mm and $s = 3$ mm).

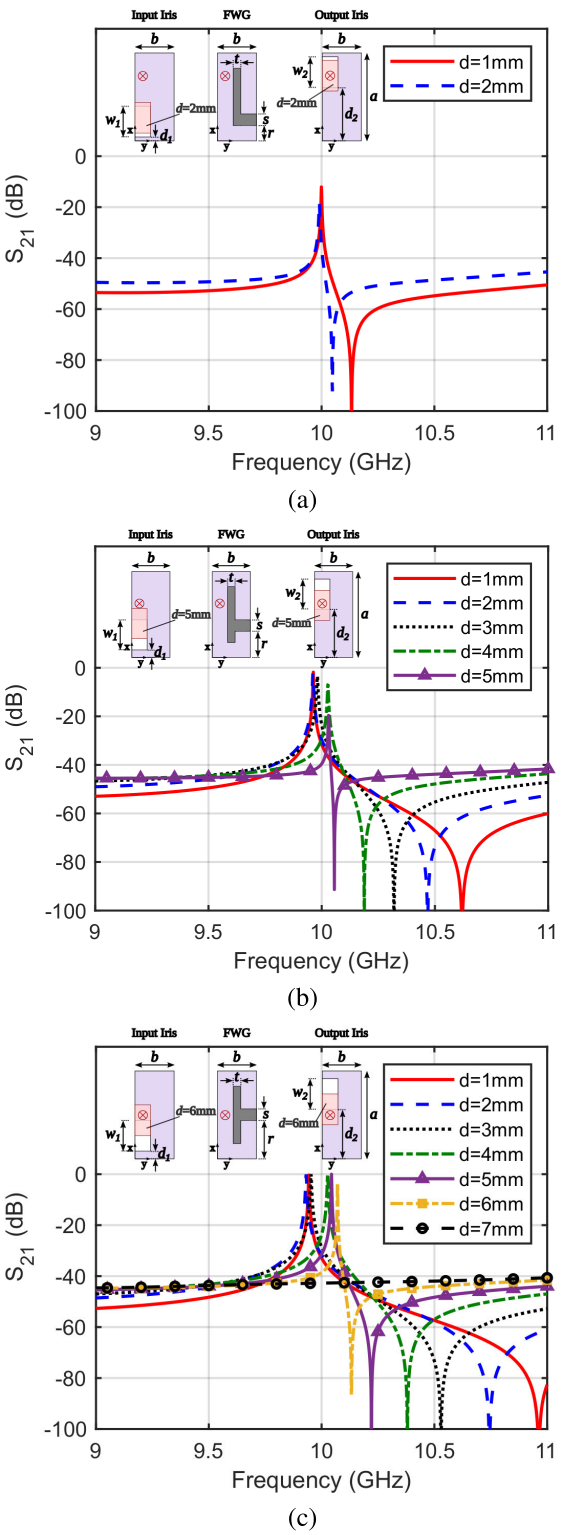

FIGURE 8. S_{21} versus d for the proposed singlet with irises on opposite sides of FWG center axis for (a) $r = 4$ mm, (b) $r = 7$ mm, and (c) $r = 10$ mm. Insets of (a), (b) and (c) show the cross-sectional views of input iris, FWG cavity resonator and output iris for $r = 4$ mm, 7 mm and 10 mm respectively. ($a = 22.86$ mm, $b = 10.16$ mm, $d_1 = d$, $d_2 = a - d - w_2$, $w_1 = w_2 = 8$ mm, $t = 2$ mm and $s = 3$ mm).

C. IRISES ON OPPOSITE SIDES OF FWG CENTER AXIS

For the case where input and output irises are located on opposite sides of FWG center axis [see Fig. 5(c)], a TZ above the pole can be realized. Note that the magnetic field lines for the non-resonating (dominant) and the resonant (first higher order) modes are out of phase at the output of the singlet of Fig. 5(c), hence creating a TZ in the upper stopband. We can adjust the location of TZ by changing dimension d_1 for input and d_2 for output irises, as shown in Fig. 8. Here all coupling coefficients namely M_{S1}, M_{SL} and M_{1L} are non-zero because the feeding TE_{10} mode of rectangular waveguide can excite both dominant and first higher order modes of FWG.

Note that Fig. 8 shows the singlet for which parameter d_1 of input and d_2 of output are set in terms of a new parameter d, as $d_1 = d$ and $d_2 = a - d - w_2$. The insets show the cross-sectional views at different locations of the singlet structure. Fig. 8(a) shows the singlet response for $r = 4$ mm. Here only $d = 1$ mm and $d = 2$ mm are shown, because when d becomes further greater, the irises are no longer on opposite sides of FWG center axis and will therefore realize TZ below the passband instead (see subsection II-B).

Fig. 8(b) shows TZs implemented above passband when $r = 7$ mm. Here d can become as large as 5 mm. Fig. 8(c) represents the responses for $r = 10$ mm. This case gives the widest range for variation in dimension d, to realize a TZ at the required location in the upper stopband. d value close to 7 mm results in the case of subsection II-A, thus producing neither a pole nor a TZ.

It is worth mentioning, that for ease of explanation, dimensions d_1 of input iris and d_2 of output iris have been expressed in terms of a variable d ($d_1 = d$ and $d_2 = a - d - w_2$). However, this constraint is not required by the structure and the two parameters can be set independently of each other, thus giving more flexibility in implementation of the desired singlet response.

III. THREE-POLE/ONE-TZ WAVEGUIDE FILTER

Higher order filters can be designed by cascading multiple singlets or by cascading a combination of singlets and resonators [19], [24], [34]. In this section, a three-pole filter with one TZ below the passband is designed. The TZ below the passband is realized by using the singlet with irises on same side of FWG center axis [see Fig. 5(b)]. For this filter, the remaining two poles are realized by using FWG cavity resonators operating in dominant TE_{101} like mode. Fig. 9 shows the routing and coupling scheme for this three-pole filter. The CM is of the form

$$M = \begin{bmatrix} 0 & M_{S1} & 0 & 0 & 0 \\ M_{S1} & M_{11} & M_{12} & M_{13} & 0 \\ 0 & M_{12} & M_{22} & M_{23} & 0 \\ 0 & M_{13} & M_{23} & M_{33} & M_{3L} \\ 0 & 0 & 0 & M_{3L} & 0 \end{bmatrix} \quad (2)$$

Optimization based technique [35] is utilized to synthesize the CM for the required filter response. Fig. 10 shows the CM response. The synthesized CM is given below in (3).

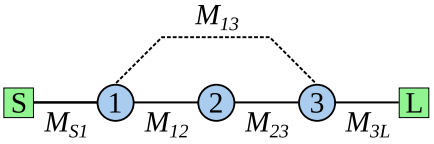

FIGURE 9. Routing and coupling scheme for the three-pole/one-TZ waveguide filter.

TABLE 1. Resonant frequencies computed from the CM representation of the designed three-pole/one-TZ waveguide filter.

i	M_{ii}	f_r^i (GHz)
1	-0.1426	10.2214
2	0.6074	10.1093
3	-0.1426	10.2214

TABLE 2. Synthesized equivalent circuit parameter values for the designed three-pole/one-TZ waveguide filter.

Parameter	Value
K_{S1}	0.2471
K_{3L}	0.2471
ℓ_1	15.57 mm
ℓ_3	15.57 mm
$M^{(S2)}$	$\begin{bmatrix} 0 & 0.0344 & -0.0332 \\ 0.0344 & 0.0180 & 0.0344 \\ -0.0332 & 0.0344 & 0 \end{bmatrix}$

$$M = \begin{bmatrix} 0 & 1.0832 & 0 & 0 & 0 \\ 1.0832 & -0.1426 & 0.8788 & -0.6345 & 0 \\ 0 & 0.8788 & 0.6074 & 0.8788 & 0 \\ 0 & -0.6345 & 0.8788 & -0.1426 & 1.0832 \\ 0 & 0 & 0 & 1.0832 & 0 \end{bmatrix} \quad (3)$$

where computed values of M_{11}, M_{22} and M_{33} can be used to determine the resonant frequencies of FWG1, singlet (S2) and FWG3 section, respectively using the equation below [24], [34].

$$f_r^i = 0.5 f_0 \left[\sqrt{(M_{ii} \times FBW)^2 + 4} - M_{ii} \times FBW \right] \quad (4)$$

where f_0 is the center frequency and FBW is the fractional bandwidth. For this design $f_0 = 10.2$ GHz and $FBW = 0.3/10.2 = 0.0294$. The resulting resonant frequencies are as given in Table 1. Note that the positive values of M_{ii} leads to resonant frequencies smaller than f_0 while negative values of M_{ii} results in resonant frequencies greater than f_0.

To design this filter from the CM (3), an equivalent circuit shown in Fig. 11 has been synthesized using a procedure similar to [25]. The equivalent circuit consists of input and output couplings (K_{S1} and K_{3L}), singlet (S2) represented by its CM and folded waveguide sections operating in dominant resonant modes (FWG_1 and FWG_3 of lengths ℓ_1 and ℓ_3, respectively). Basic microwave network theory [36] has been utilized to represent each block of Fig. 11 as an ABCD matrix.

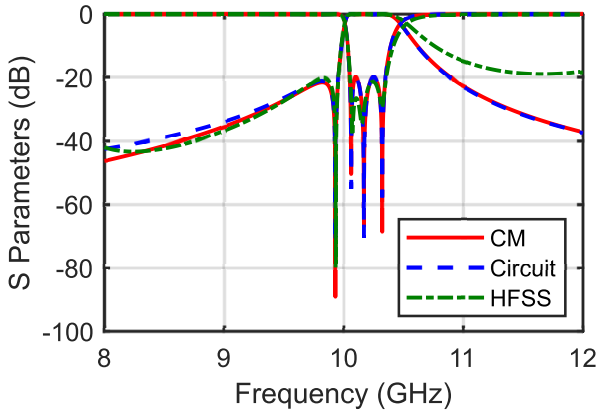

FIGURE 10. Coupling matrix (CM), equivalent circuit and HFSS simulation responses for the three-pole/one-TZ waveguide filter.

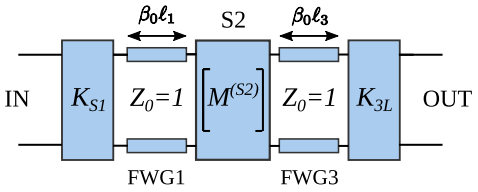

FIGURE 11. Equivalent circuit for the three-pole/one-TZ waveguide filter.

The individual ABCD matrices are then multiplied to obtain the overall ABCD matrix of the filter.

$$ABCD_{Filter} = ABCD_{KS1} \times ABCD_{FWG1} \times ABCD_{S2} \times ABCD_{FWG3} \times ABCD_{K3L} \quad (5)$$

where ABCD matrices for input coupling, output coupling and FWG sections operating in dominant mode can be given as [36], [37]

$$ABCD_{KS1} = \begin{bmatrix} 0 & jK_{S1} \\ j/K_{S1} & 0 \end{bmatrix}$$

$$ABCD_{K3L} = \begin{bmatrix} 0 & jK_{3L} \\ j/K_{3L} & 0 \end{bmatrix}$$

$$ABCD_{FWG1} = \begin{bmatrix} cos(\beta\ell_1) & jsin(\beta\ell_1) \\ jsin(\beta\ell_1) & cos(\beta\ell_1) \end{bmatrix}$$

$$ABCD_{FWG3} = \begin{bmatrix} cos(\beta\ell_3) & jsin(\beta\ell_3) \\ jsin(\beta\ell_3) & cos(\beta\ell_3) \end{bmatrix}$$

where β is the propagation constant of the dominant (TE_{10} like) mode in each FWG section.

Singlet S-parameters are determined from its CM of (1), using equations from [35] and using unity fractional bandwidth ($FBW = 1$). These S-parameters are converted in to the required ABCD matrix by using the standard conversion tables [36]. The complete equivalent circuit of Fig. 11 is then synthesized using optimization based method [25], [35]. The required design parameters to be synthesized are given as the vector below

$$x = \left[K_{S1}\ \beta_0\ell_1\ M_{S1}^{(S2)}\ M_{SL}^{(S2)}\ M_{11}^{(S2)}\ M_{1L}^{(S2)}\ \beta_0\ell_3\ K_{3L} \right] \quad (6)$$

The objective function used is given in (7), where ABCD parameters are determined for each iteration and each frequency point, using (5) and then ABCD to S-parameter conversion is carried out to obtain the overall S-parameters [25].

$$\Psi = \sum_{u=1}^{N} W_{pu} \left| S_{11}\left(f_{pu}\right) \right|^2 + \sum_{v=1}^{M} W_{zv} \left| S_{21}\left(f_{zv}\right) \right|^2 + \sum_{w=1}^{N+1} \left(\left| S_{11}\left(f_w\right) \right| - 10^{-RL/20} \right)^2 \quad (7)$$

where f_{pu} and f_{zv} represent the desired poles and TZs frequencies, respectively. W_{pu} and W_{zv} are the weights for poles and TZs, respectively. These weights may be adjusted to give more importance to some terms in the objective function. For this filter design, $W_{pu} = 1$ and $W_{zv} = 100$ have been used. RL indicates the required passband return loss of the filter. f_1 and f_2 are the frequency points defined at the edges of the passband. f_3 and f_4 are additional frequency points at which RL has the same value as that at the edge frequency points. N is the number of poles and M is the number of TZs. For this three-pole filter $f_1 = 10.05$ GHz, $f_2 = 10.35$ GHz, $f_3 = 10.104$ GHz, $f_4 = 10.254$ GHz, $N = 3$, $M = 1$ and $RL = 20$ dB.

The synthesized equivalent circuit parameters are given in Table 2.

Fig. 10 shows the frequency response for the synthesized equivalent circuit, and it agrees well with the CM response. Using the synthesized equivalent circuit of Table 2, the physical dimensions of the filter can be obtained. Iris widths of the input and output irises can be determined from the values of K_{S1} and K_{3L}, respectively, using the well-known waveguide iris filter design method [38]. The physical lengths for the two FWG sections (ℓ_1 and ℓ_3) are already determined and are given in Table 2. To determine the physical dimensions of the singlet S2 (shown in Fig. 1), full wave electromagnetic (EM) simulations are carried out to achieve a close match of the simulated S-parameter response to that of the singlet CM. Fig. 12 compares the coupling matrix response with the simulation response, which indicates the two responses are almost similar particularly in the vicinity of the pole and the TZ. The phase response of the simulated singlet is then matched to that of the singlet CM to determine the locations of the input/output reference planes for the simulated singlet structure.

The resulting dimensions are then used to create the filter structure in HFSS. Some optimizations are required in this full wave EM simulator, since the equivalent circuit model does not account for all the higher-order mode effects. Optimizations are performed in HFSS and the resulting response is plotted in Fig. 10, which indicates that the HFSS response is in good agreement with the CM and circuit responses.

Manufacturing of the designed three-pole filter is carried out by CNC milling of aluminum. The manufactured prototype filter is shown in Fig. 13.

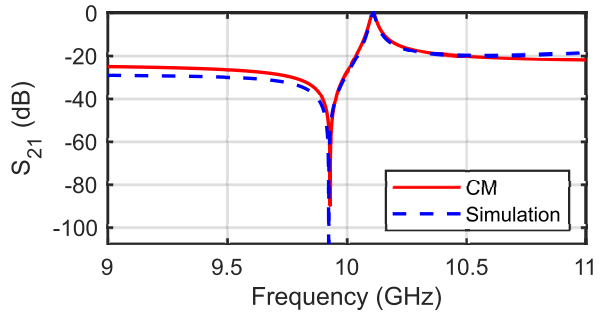

FIGURE 12. CM and simulation responses of the singlet S2.

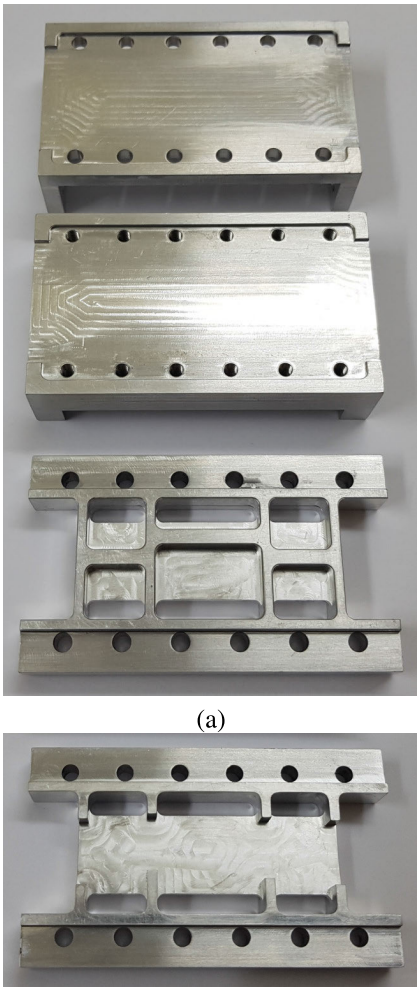

FIGURE 13. Manufactured prototype of the three-pole/one-TZ waveguide filter. (a) Top view with two lids, and (b) bottom view.

A vector network analyzer is used to measure the S-parameter response of the manufactured prototype. The measured results along with HFSS simulation results are plotted in Fig. 14. These results show a good agreement of the measured S-parameters to the simulated response. Measured in-band return loss is better than 16.48 dB. Measured half-power bandwidth is 492.2 MHz against the simulated

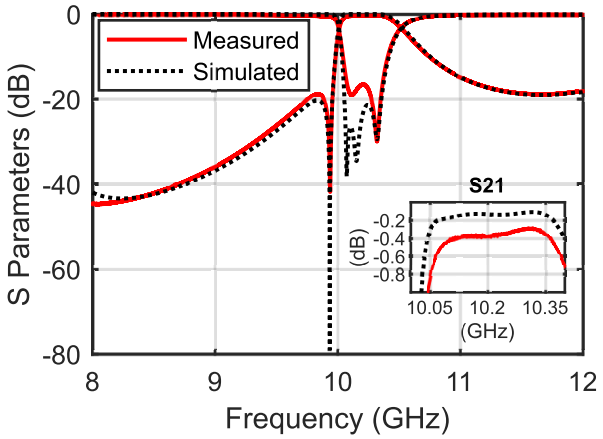

FIGURE 14. Measured and HFSS responses of the three-pole/one-TZ waveguide filter.

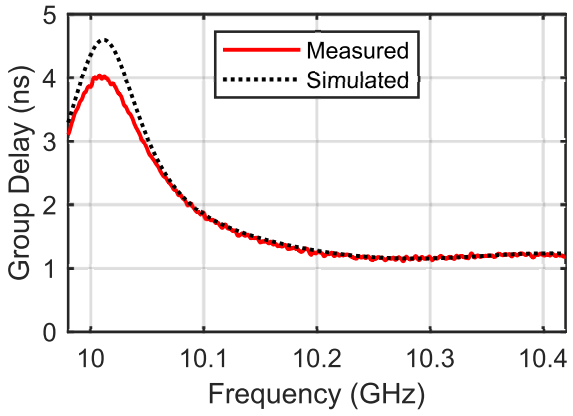

FIGURE 15. Measured and simulated group delay responses of the three-pole/one-TZ waveguide filter.

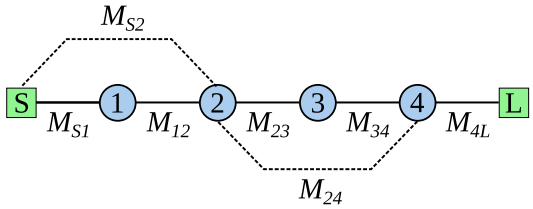

FIGURE 16. Routing and coupling scheme for the four-pole/two-TZ waveguide filter.

value of 520 MHz. The inset of Fig. 21 also shows the close-up view of the measured in-band insertion loss (IL). At center frequency of 10.2 GHz, the measured IL is 0.375 dB instead of the simulated value of 0.134 dB. The measured and simulated in-band group delay responses are compared in Fig. 15.

IV. FOUR-POLE/TWO-TZ WAVEGUIDE FILTER

A four-pole pseudo-elliptic waveguide filter with two TZs, one above and another below the passband is designed by using two singlets and two half-wave rectangular waveguide sections. The singlet implementing lower stopband TZ makes use of irises on same side of FWG center axis [see fig 5(b)]

TABLE 3. Resonant frequencies computed from the CM representation of the designed four-pole/two-TZ waveguide filter.

i	M_{ii}	f_r^i (GHz)
1	-0.7159	10.3080
2	0.2461	10.1632
3	0.6086	10.1091
4	-0.0079	10.2012

while the singlet realizing upper stopband TZ utilizes irises on opposite sides of FWG center axis [see fig 5(c)].

The routing and coupling scheme for this four-pole filter is shown in Fig. 16.

A 6×6 CM of the form below, can be used to represent this filter response.

$$M = \begin{bmatrix} 0 & M_{S1} & M_{S2} & 0 & 0 & 0 \\ M_{S1} & M_{11} & M_{12} & 0 & 0 & 0 \\ M_{S2} & M_{12} & M_{22} & M_{23} & M_{24} & 0 \\ 0 & 0 & M_{23} & M_{33} & M_{34} & 0 \\ 0 & 0 & M_{24} & M_{34} & M_{44} & M_{4L} \\ 0 & 0 & 0 & 0 & M_{4L} & 0 \end{bmatrix} \tag{8}$$

To synthesize this CM, same methodology as explained in Section III is utilized. The resulting CM is shown below as (9).

$$M = \begin{bmatrix} 0 & 0.9355 & 0.4262 & 0 & 0 & 0 \\ 0.9355 & -0.7159 & 0.7193 & 0 & 0 & 0 \\ 0.4262 & 0.7193 & 0.2461 & 0.6090 & -0.4372 & 0 \\ 0 & 0 & 0.6090 & 0.6086 & 0.7746 & 0 \\ 0 & 0 & -0.4372 & 0.7746 & -0.0079 & 1.0260 \\ 0 & 0 & 0 & 0 & 1.0260 & 0 \end{bmatrix} \tag{9}$$

where synthesized values of M_{11}, M_{22}, M_{33} and M_{44} can be utilized to determine the resonant frequencies of singlet (S1), waveguide section (WG2), singlet (S3) and waveguide section (WG4), respectively using (4). The resulting resonant frequencies are as shown in Table 3. It is worth mentioning that the positive values of M_{ii} result in resonant frequencies smaller than f_0 while the negative values of M_{ii} lead to resonant frequencies larger than f_0. For this filter, $f_0 = 10.2$ GHz.

The S-parameter response of the CM of (9) is given in Fig. 17. The equivalent circuit of Fig. 18 is utilized to design this filter. The design procedure is optimization based and is similar to the one explained in Section III. ABCD matrices are utilized to represent each block of the equivalent circuit. Table 4 shows the synthesized parameters for the equivalent circuit of Fig. 18.

For each singlet (S1 and S3), the S-parameter response of the CM [see Table 4] is matched to that of the physical structure using HFSS. The comparison of CM response with full wave simulation response for each singlet is shown in Fig. 19. The simulated response compares well with the CM response for each singlet in the vicinity of pole and TZ locations. Using the same steps as in Section III, the resulting dimensions are implemented in HFSS for this four-pole filter. The simulated S-parameter response is shown in Fig. 17, which also compares it with CM and circuit responses. The simulated response is in good agreement with the CM and

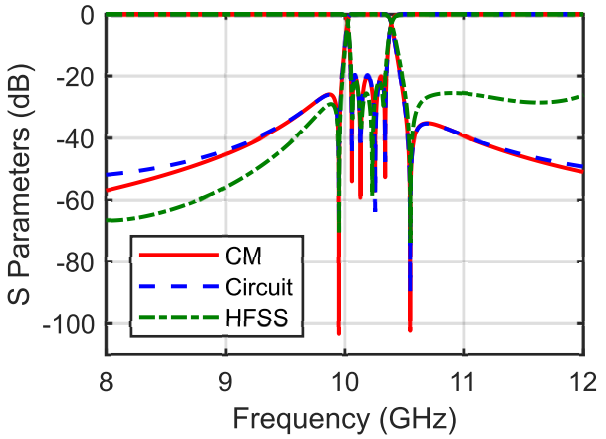

FIGURE 17. Coupling matrix (CM), equivalent circuit and HFSS simulation responses for the four-pole/two-TZ waveguide filter.

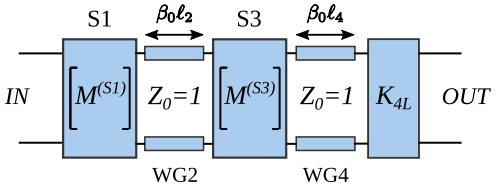

FIGURE 18. Equivalent circuit for the four-pole/two-TZ waveguide filter.

TABLE 4. Synthesized equivalent circuit parameter values for the designed four-pole/two-TZ waveguide filter.

Parameter	Value
ℓ_2	19.302 mm
ℓ_4	19.179 mm
K_{4L}	0.2851
$M^{(S1)}$	$\begin{bmatrix} 0 & 0.1600 & 0.1193 \\ 0.1600 & -0.0211 & 0.0346 \\ 0.1193 & 0.0346 & 0 \end{bmatrix}$
$M^{(S3)}$	$\begin{bmatrix} 0 & 0.0293 & -0.0341 \\ 0.0293 & 0.0178 & 0.0371 \\ -0.0341 & 0.0371 & 0 \end{bmatrix}$

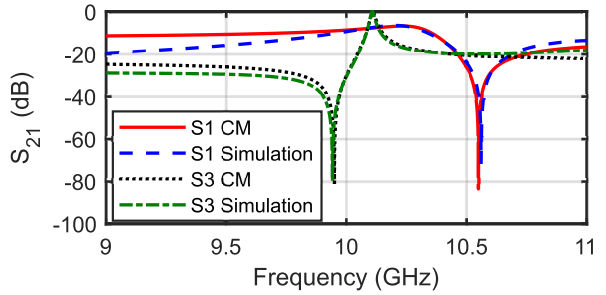

FIGURE 19. CM and simulation responses of the two singlets (S1 and S3).

TABLE 5. Comparison with previously reported waveguide pseudo-elliptic filters based on the concept of non-resonating modes.

Topology	Basic Structure	Resonating Mode	Non-resonating Mode	Number of Poles	Number of TZs	Measured In-band RL (dB)	Measured IL at center frequency (dB)	Cross-sectional size relative to standard waveguide	Manufacturing Difficulty/ Tuning Effort	Estimated Q_u from measured Results
Singlet [16]–[18]	H-plane enlarged width rectangular waveguide cavity	TE_{201}	TE_{10}	3 5	1 3	>13 >16	0.38 N/A	Larger	Low	N/A
Singlet [20]	TM mode rectangular waveguide cavity	TM_{110}	TE_{10}	4	3	>20	0.4	Larger	Low	N/A
Doublet [21], [22]	TM dual-mode rectangular waveguide cavity	TM_{120}, TM_{210}	TM_{11}	8	8	>16	0.6	Larger	High	4500
Singlet [24]	Slant and transverse rectangular ridge	Ridge parallel plate mode	TE_{10}	5	3	>16	0.35	Same	Low	N/A
Singlet [25]	Transverse rectangular ridge with asymmetric irises	Ridge parallel plate mode	TE_{10}	3 5	1 2	>22 >10.38	0.28 0.862	Same	Low	1363[a] 3680[b]
Singlet [26], [27]	Dielectric disks in propagating rectangular waveguide	$TE_{01\delta}$	TE_{10}	3	3	>16.5	N/A	Same	High	5000
Singlet and doublet [28]	Dual-post	Odd symmetry mode of a dual-post resonator	TE_{10}	6	6	>18	0.55	Same	Medium	2300
Singlet This Work	Iris-coupled Folded-waveguide (FWG) cavity	TE_{201} like mode of FWG	TE_{10}	3 4	1 2	>16.48 >19.16	0.375 0.319	Same	Low	1500[a] 2795[b]

N/A: Not available, RL: Return Loss, IL: Insertion Loss.

[a]Unloaded quality factor of singlet. [b]Unloaded quality factor of waveguide section.

circuit responses particularly in close proximity of the passband and TZs locations.

Manufacturing of the filter is carried out using CNC milling and the manufactured prototype is shown in Fig. 20.

The filter's measured response is shown in Fig. 21, which also shows the HFSS simulated response. The measured S-parameters match well with the simulated results. The measured return loss is better than 19.16 dB in the passband. Tolerance analysis is performed in HFSS using a Gaussian distribution with standard deviation of 10 μm. For each iteration, all physical dimensions of the filter except for a and b of the waveguide are randomly varied and the results of 50 such iterations are shown as gray lines in Fig. 21. It is observed that the locations of TZs are insensitive to the manufacturing errors while the return loss is slightly affected by these errors. The worst case passband return loss is 15.68 dB, making this filter suitable for use without the need of any tuning mechanism.

The close-up view of the in-band insertion loss (IL) is shown in the inset of Fig. 21. Measured IL is 0.319 dB at 10.2 GHz in contrast to the simulated value of 0.156 dB. From the measured IL, the unloaded quality factor for each singlet is estimated as $Q_u^{Singlet} = 1500$ and for each waveguide section as $Q_u^{WG} = 2795$. Measured half-power bandwidth is 360.9 MHz while the simulated value is 369.5 MHz. The measured and simulated in-band group delay responses are shown in Fig. 22.

Table 5 compares the proposed structure with other previously reported non-resonating modes based waveguide pseudo-elliptic filters. The proposed filters are easily

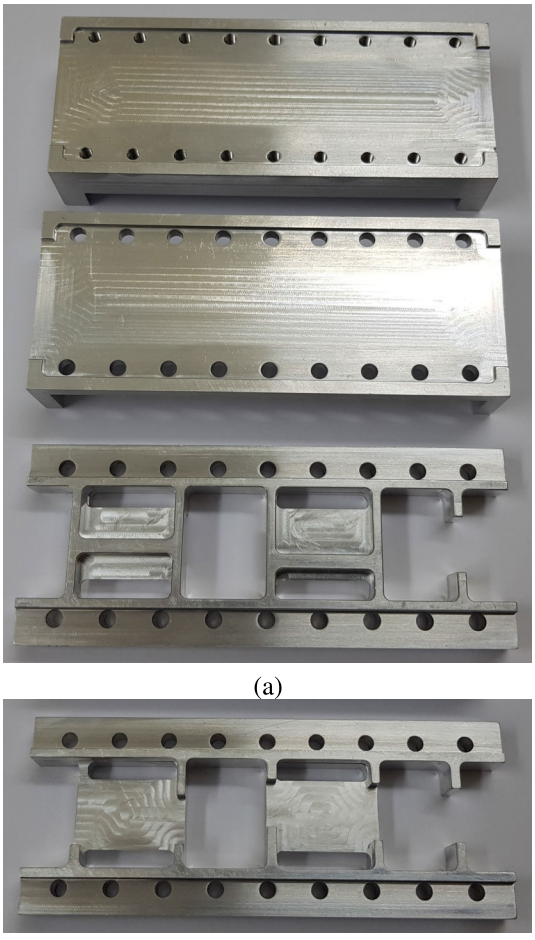

FIGURE 20. Manufactured prototype of the four-pole/two-TZ waveguide filter. (a) Top view with lids, and (b) bottom view.

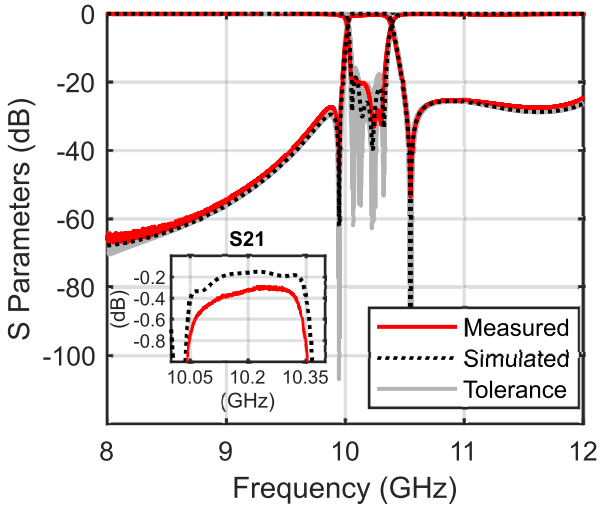

FIGURE 21. Measured and HFSS responses of the four-pole/two-TZ waveguide filter.

manufactured through CNC milling, are less sensitive to manufacturing errors, do not exceed the cross-sectional area dimensions of the feeding rectangular waveguides and achieve good unloaded quality factors and insertion loss.

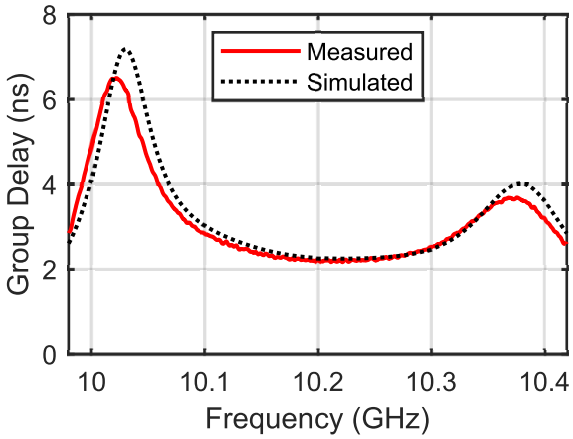

FIGURE 22. Measured and simulated group delay responses of the four-pole/two-TZ waveguide filter.

V. CONCLUSION

A new class of inline waveguide pseudo-elliptic filters, using a novel singlet structure based on folded-waveguide (FWG) cavity resonator has been presented in this work. The FWG is fed by rectangular waveguides using irises that excite both resonant and non-resonating modes. The dimensions and locations of the irises are adjusted to achieve the required location of TZs. Proper placement of input and output irises relative to each other and relative to the FWG center axis, leads to an implementation of a TZ either below or above the passband. Additionally, FWG center axis may also be adjusted thus providing more flexibility in realizing the required singlet response.

The proposed singlet structures have been used to design a three-pole filter with one TZ below the passband and a four-pole filter with two TZs, one below and other above the passband. Manufacturing tolerance analysis of the four-pole filter indicates that the filter performance is not very sensitive to manufacturing errors, with worst-case return loss of 15.68 dB and TZs locations almost the same as their designed locations. The two prototype filters are manufactured through CNC milling process and measured using a vector network analyzer. The measurements show a good consistency with the simulated data, thus verifying the practicality of the proposed singlet structure and the resulting filters.

REFERENCES

[1] R. V. Snyder, A. Mortazawi, I. Hunter, S. Bastioli, G. Macchiarella, and K. Wu, "Present and future trends in filters and multiplexers," *IEEE Trans. Microw. Theory Techn.*, vol. 63, no. 10, pp. 3324–3360, Oct. 2015.

[2] R. V. Snyder, G. Macchiarella, S. Bastioli, and C. Tomassoni, "Emerging trends in techniques and technology as applied to filter design," *IEEE J. Microw.*, vol. 1, no. 1, pp. 317–344, 2021.

[3] V. E. Boria and B. Gimeno, "Waveguide filters for satellites," *IEEE Microw. Mag.*, vol. 8, no. 5, pp. 60–70, Oct. 2007.

[4] A. E. Williams, "A four-cavity elliptic waveguide filter," *IEEE Trans. Microw. Theory Techn.*, vol. MTT-18, no. 12, pp. 1109–1114, Dec. 1970.

[5] A. Atia and A. Williams, "New types of waveguide bandpass filters for satellite transponders," *Comsat Tech. Rev.*, vol. 1, no. 1, pp. 20–43, 1971.

[6] A. E. Atia and A. E. Williams, "Nonminimum-phase optimum-amplitude bandpass waveguide filters," *IEEE Trans. Microw. Theory Techn.*, vol. MTT-22, no. 4, pp. 425–431, Apr. 1974.

[7] W.-C. Tang and S. K. Chaudhuri, "A true elliptic-function filter using triple-mode degenerate cavities," *IEEE Trans. Microw. Theory Techn.*, vol. MTT-32, no. 11, pp. 1449–1454, Nov. 1984.
[8] R. R. Bonetti and A. E. Williams, "Application of dual TM modesto Triple- and quadruple-mode filters," *IEEE Trans. Microw. Theory Techn.*, vol. MTT-35, no. 12, pp. 1143–1149, Dec. 1987.
[9] M. Guglielmi, P. Jarry, E. Kerherve, O. Roquebrun, and D. Schmitt, "A new family of all-inductive dual-mode filters," *IEEE Trans. Microw. Theory Techn.*, vol. 49, no. 10, pp. 1764–1769, Oct. 2001.
[10] J. D. Rhodes and R. J. Cameron, "General extracted pole synthesis technique with applications to low-loss TE_{011} mode filters," *IEEE Trans. Microw. Theory Tech.*, vol. MTT-28, no. 9, pp. 1018–1028, Sep. 1980.
[11] S. Amari and J. Bornemann, "Using frequency-dependent coupling to generate finite attenuation poles in direct-coupled resonator bandpass filters," *IEEE Microw. Guided Wave Lett.*, vol. 9, no. 10, pp. 404–406, Oct. 1999.
[12] S. Bastioli, "Nonresonating mode waveguide filters," *IEEE Microw. Mag.*, vol. 12, no. 6, pp. 77–86, Oct. 2011.
[13] S. Bastioli and R. V. Snyder, "Nonresonating modes do it better!: Exploiting additional modes in conjunction with operating modes to design better quality filters," *IEEE Microw. Mag.*, vol. 22, no. 1, pp. 20–45, Jan. 2021.
[14] F. Arndt, T. Duschak, U. Papziner, and P. Rolappe, "Asymmetric iris coupled cavity filters with stopband poles," in *IEEE MTT-S Int. Microw. Symp. Dig.*, vol. 1, May 1990, pp. 215–218.
[15] M. Guglielmi, F. Montauti, L. Pellegrini, and P. Arcioni, "Implementing transmission zeros in inductive-window bandpass filters," *IEEE Trans. Microw. Theory Techn.*, vol. 43, no. 8, pp. 1911–1915, Aug. 1995.
[16] G. Iguchi, M. Tsuji, and H. Shigesawa, "Negative coupling between TE_{10} and TE_{20} modes for use in evanescent-mode bandpass filters and their field-theoretic CAD," in *IEEE MTT-S Int. Microw. Symp. Dig.*, vol. 2, May 1994, pp. 727–730.
[17] S. Amari and U. Rosenberg, "Characteristics of cross (bypass) coupling through higher/lower order modes and their applications in elliptic filter design," *IEEE Trans. Microw. Theory Techn.*, vol. 53, no. 10, pp. 3135–3141, Oct. 2005.
[18] G. Macchiarella, G. G. Gentili, C. Tomassoni, S. Bastioli, and R. V. Snyder, "Design of waveguide filters with cascaded singlets through a synthesis-based approach," *IEEE Trans. Microw. Theory Techn.*, vol. 68, no. 6, pp. 2308–2319, Jun. 2020.
[19] S. Amari, U. Rosenberg, and J. Bornemann, "Singlets, cascaded singlets, and the nonresonating node model for advanced modular design of elliptic filters," *IEEE Microw. Wireless Compon. Lett.*, vol. 14, no. 5, pp. 237–239, May 2004.
[20] U. Rosenberg, S. Amari, and J. Bornemann, "Inline TM_{110}-mode filters with high-design flexibility by utilizing bypass couplings of nonresonating $TE_{10/01}$ modes," *IEEE Trans. Microw. Theory Tech.*, vol. 51, no. 6, pp. 1735–1742, Jun. 2003.
[21] S. Bastioli, C. Tomassoni, and R. Sorrentino, "A new class of waveguide dual-mode filters using TM and nonresonating modes," *IEEE Trans. Microw. Theory Techn.*, vol. 58, no. 12, pp. 3909–3917, Dec. 2010.
[22] C. Tomassoni, S. Bastioli, and R. Sorrentino, "Generalized TM dual-mode cavity filters," *IEEE Trans. Microw. Theory Techn.*, vol. 59, no. 12, pp. 3338–3346, Dec. 2011.
[23] L. Pelliccia, F. Cacciamani, C. Tomassoni, and R. Sorrentino, "Ultra-compact high-performance filters based on TM dual-mode dielectric-loaded cavities," *Int. J. Microw. Wireless Technol.*, vol. 6, no. 2, pp. 151–159, Apr. 2014.
[24] S. Bastioli, C. Marcaccioli, and R. Sorrentino, "Waveguide pseudoelliptic filters using slant and transverse rectangular ridge resonators," *IEEE Trans. Microw. Theory Techn.*, vol. 56, no. 12, pp. 3129–3136, Dec. 2008.
[25] M. A. Chaudhary and M. M. Ahmed, "Inline pseudoelliptic waveguide filters using asymmetric iris coupled transverse rectangular ridge resonators," *Int. J. Microw. Wireless Technol.*, vol. 4, pp. 1–9, Apr. 2021.
[26] C. Tomassoni, S. Bastioli, and R. V. Snyder, "Propagating waveguide filters using dielectric resonators," *IEEE Trans. Microw. Theory Techn.*, vol. 63, no. 12, pp. 4366–4375, Dec. 2015.
[27] C. Tomassoni, S. Bastioli, and R. V. Snyder, "Pseudo-elliptic in-line filters with dielectric resonators in propagating waveguide," in *IEEE MTT-S Int. Microw. Symp. Dig.*, May 2015, pp. 1–4.
[28] C. Tomassoni and R. Sorrentino, "A new class of pseudoelliptic waveguide filters using dual-post resonators," *IEEE Trans. Microw. Theory Techn.*, vol. 61, no. 6, pp. 2332–2339, Jun. 2013.
[29] Y. Xiao, P. Shan, K. Zhu, H. Sun, and F. Yang, "Analysis of a novel singlet and its application in THz bandpass filter design," *IEEE Trans. THz Sci. Technol.*, vol. 8, no. 3, pp. 312–320, 2018.
[30] N. Grigoropoulos and P. R. Young, "Compact folded waveguides," in *Proc. 34th Eur. Microw. Conf.*, vol. 2, Oct. 2004, pp. 973–976.
[31] G. H. Zhai, W. Hong, K. Wu, J. X. Chen, P. Chen, J. Wei, and H. J. Tang, "Folded half mode substrate integrated waveguide 3 dB coupler," *IEEE Microw. Wireless Compon. Lett.*, vol. 18, no. 8, pp. 512–514, Aug. 2008.
[32] D.-W. Kim and J.-H. Lee, "Partial H-plane filters with partially inserted H-plane metal vane," *IEEE Microw. Wireless Compon. Lett.*, vol. 15, no. 5, pp. 351–353, May 2005.
[33] D.-W. Kim, D.-J. Kim, and J.-H. Lee, "Compact partial H-plane filters," *IEEE Trans. Microw. Theory Tech.*, vol. 54, no. 11, pp. 3923–3930, 2006.
[34] G. Macchiarella, "Generalized coupling coefficient for filters with non-resonant nodes," *IEEE Microw. Wireless Compon. Lett.*, vol. 18, no. 12, pp. 773–775, Dec. 2008.
[35] S. Amari, U. Rosenberg, and J. Bornemann, "Adaptive synthesis and design of resonator filters with source/load-multiresonator coupling," *IEEE Trans. Microw. Theory Techn.*, vol. 50, no. 8, pp. 1969–1978, Aug. 2002.
[36] D. M. Pozar, *Microwave Engineering*. Hoboken, NJ, USA: Wiley, 2011.
[37] J.-S. Hong, *Microstrip Filters for RF/Microwave Applications*. Hoboken, NJ, USA: Wiley, 2011.
[38] R. J. Cameron, R. Mansour, and C. M. Kudsia, *Microwave Filters for Communication Systems: Fundamentals, Design, and Applications*. Hoboken, NJ, USA: Wiley, 2007.

MUHAMMAD ANIS CHAUDHARY (Member, IEEE) received the B.E. and M.S. degrees in electrical engineering from the National University of Sciences & Technology (NUST), Pakistan, in 2003 and 2010, respectively. He is currently pursuing the Ph.D. degree in electrical engineering with the Capital University of Science and Technology (CUST), Islamabad, Pakistan. His research interests include microwave filters and passive structures.

MUHAMMAD MANSOOR AHMED (Senior Member, IEEE) received the Ph.D. degree in microelectronics from the University of Cambridge, U.K., in 1995. After his Ph.D. degree, he joined Academia where he worked at different positions including a Professor, the Chairman, the Dean, and the Executive Vice President. He is currently working as the Vice Chancellor of the Capital University of Science and Technology (CUST), Islamabad. He has supervised numerous M.S. and Ph.D. research projects. He has authored over 100 research papers in the field of microelectronics. His research interests include microelectronics, microwave, and RF engineering. He is a fellow of the Institution of Engineering and Technology (IET), U.K.; a Chartered Engineer (CEng) from the U.K. Engineering Council; and holds the title of European Engineer (EUR ING) from the European Federation of National Engineering Association (FEANI), Brussels. He is also a Life Member of PEC, Pakistan; EDS; and MTTS, USA.